

Methods for analytically estimating the resolution and intensity of neutron time-of-flight spectrometers.

The case of the TOFTOF spectrometer

Ana M Gaspar*

An analytical method is presented with allows to estimate the energy resolution of time-of-flight neutron spectrometers, as well as its partial contributions, over a dynamical range that extends from the elastic line to the accessible inelastic regions. Such a method, already successfully applied in the past to the TOSCA and HET neutron inelastic scattering spectrometers installed at the ISIS neutron spallation source [A M Gaspar, PhD Thesis, Universidade Tecnica de Lisboa, 2004], is here applied to the high resolution time-of-flight spectrometer TOFTOF, mainly dedicated to quasi-elastic neutron scattering studies and installed at the new neutron reactor FRM II. To make such calculations easily understandable, the principle of work of the TOFTOF instrument and of each of its components is explained in detail. A simply method that can be used to estimate the instrument intensity, i.e. of the number of neutrons arriving at the sample position per unit time, is also briefly outlined.

To the benefit of the TOFTOF users, graphs displaying the dependencies of the instrument resolution at the elastic line and of the instrument intensity on the relevant instrument parameters, i.e the wavelength of the incident neutrons, the choppers speed of rotation and the frame overlap ratio, are presented, in the form of iso-resolution or iso-intensity lines. The method of estimation of the frame overlap ratio that is commonly used at time-of-flight instruments such as TOFTOF is also explained and alternative options concerning this parameter, depending on the dynamical range of interest, are briefly addressed.

Contents

| | |
|--|----|
| I. Description of the TOFTOF spectrometer | 2 |
| A. The neutrons seen by TOFTOF | 2 |
| B. The chopper system | 2 |
| C. The detector system | 4 |
| II. Time-of-flight, energy transfer and momentum transfer | 7 |
| III. Instrument resolution | 8 |
| IV. Instrument intensity | 12 |
| Final Note | 13 |
| Acknowledgments | 13 |
| References | 13 |

*ana.gaspar@frm2.tum.de; www.ph.tum.de/~agapsar

I. DESCRIPTION OF THE TOFTOF SPECTROMETER

The TOFTOF spectrometer [1, 2, 3, 4] is constituted by two time-of-flight sections, where advantage is taken from the fact that (unlike electromagnetic waves) neutrons with different energies travel at different velocities, and hence take different times to travel a fixed distance - L . The primary section consists of a set of disc choppers, whose rotation around an horizontal axis parallel to the direction of the neutron beam allows to obtain a pulsed monochromatic beam at the sample position, the energy of the neutrons incident on the sample being basically determined by the phase difference between the first and the last pairs of choppers, located $L_0=10$ m apart. The secondary part of the spectrometer consists of an argon filled flight chamber forcing the scattered neutrons to travel a distance $L_1=4$ m between the sample and the detectors and allowing for the determination of their energy by measuring the time they take to travel that distance.

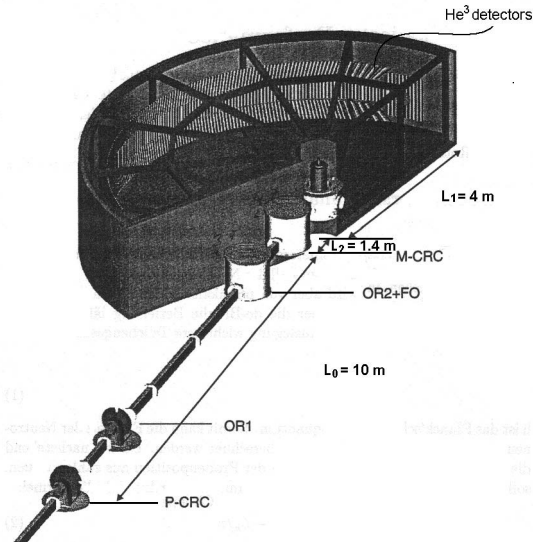


FIG. 1: Schematic representation of TOFTOF spectrometer. Figure from [2] (adapted).

A. The neutrons seen by TOFTOF

The instrument is located in the neutron-guide hall of the FRM II reactor [5] receiving moderated neutrons from its liquid deuterium cold source ($T=25\text{K}$), through an S-shaped neutron guide (of cross-section $44 \times 100 \text{ mm}^2$ and radius $\rho=2000$ m). The use of a curved S-shaped guide, which cuts-off neutrons of wavelengths smaller than 1.4\AA , ensures that the chopper system will not be irradiated with neutrons too energetic to be fully absorbed by the necessarily thin gadolinium coating of the choppers [6]. Because of that and of the aluminium windows the neutron beam must cross, the Maxwellian distribution defining the neutron flux per unit wavelength appears slightly distorted [7].

B. The chopper system

The chopper system is composed in total by seven carbon fiber composite chopper discs of diameter 600 mm, which can rotate at speeds ranging from 3000 up to 27000 rpm (50 - 450Hz). Each of these chopper discs contains one or several slits, through which neutrons will be able to pass, whereas neutrons hitting the other parts of the chopper discs will be absorbed.

The first two chopper discs form a counter-rotating (CR) pair, responsible for pulsing the incident beam, while the last two (also forming a CR pair of chopper discs) will monochromatize the neutron pulses, by choosing a specific time delay of their opening time with regards to the opening time of the pulsing pair of choppers. The main advantage of the use of a CR pair of choppers is that of allowing for a doubling of the transmitted intensity for the same opening time, when compared to single choppers (since, given the doubling of the relative speed of the slits, the CR choppers slit width may be the double of that of a single chopper)[8, 9].

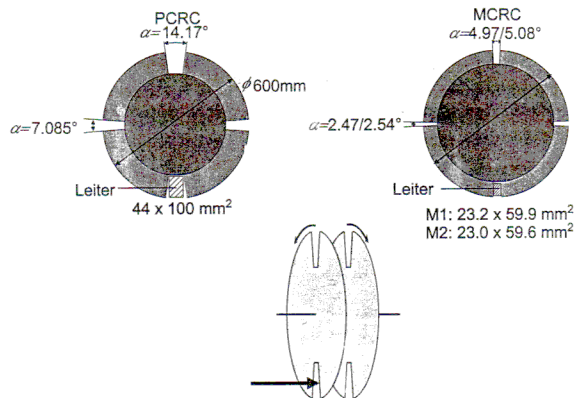


FIG. 2: Schematic representation of TOFTOF's Pulsing and Monochromating choppers with indication of the widths of their slits. Figure from [2].

The time FWHH of the transmission function of the counter-rotating pair of choppers may be approximately expressed by¹

$$\Delta t = \frac{b}{2\pi f D} \quad (1)$$

where b represents the choppers slit width, f the choppers frequency of rotation and D the choppers diameter.

Both the pulsing and the monochromating pairs of choppers contain four slits located at 90° as displayed in figure 4. Of the neutron pulses produced by passing through each of these two pairs of opposite slits only the ones created by one of them (either the larger or the smaller ones) are allowed to proceed to the sample, by means of the use of two other chopper discs located after the pulsing pair of choppers and before the monochromating pair of choppers. These two choppers also guarantee the uniqueness of the energy to be selected by the monochromating pair of choppers (and for that reason are called Order Removal choppers).

Finally, a seventh chopper, located in between the order removal choppers defines the so-called frameoverlap ratio, i.e., the portion of pulses generated by the first pair of choppers that are allowed to proceed to the last pair of choppers, and hence to the sample (1, 1/2, 1/3, 1/4, ...), by spinning at a speed that is a fraction of the speed of the other choppers. This last chopper is then the chopper that defines the repetition rate of the neutron pulses impinging on the sample and hence the maximum time window for analyzing the scattering of neutrons from one pulse, as a function of time-of-flight (hence of energy transfer), before the scattering from another pulse comes into play.

For instance, choppers spinning at 15000 rpm generate 500 neutron pulses per second, the time separating two neutron pulses being therefore 2 ms. Assuming that this time window of observation is centered around the elastic line, if using incident neutrons of 5 meV ($\lambda=4\text{\AA}$), one would only be able to obtain the spectrum of the neutrons scattered with energies between 3.2meV and 8.7 meV (hence corresponding to the range from -3.7023 to +1.7 meV in energy transfer). If, however, one would increase the time of observation to 6 ms by choosing a frameoverlap ratio equal to 3 (and hence disregarding every two out of three neutrons), one would already be able to count the neutrons

¹ The time uncertainties, are in practice commonly defined by the full width at half-height (FWHH) of the time distributions. A generally used method, which was also applied in the analysis here presented, is to approximate the distributions to Gaussians with the same root mean square deviation. In this case, the FWHH can be obtained analytically and is simply given by $\Delta t = \sqrt{8\ln(2)} \sigma_t$. Gaussians have the useful property that they may be convoluted simply by taking the root of the sums of the squares of their widths ($\sigma_t = \sqrt{\sigma_{t1}^2 + \sigma_{t2}^2 + \dots}$), which avoids the need to perform the convolution integrals and gives very similar final results. In the case of a triangular distribution as the one expected to be the transmission function of the rotating choppers, one has $\sigma_\Delta = FWHM_\Delta/\sqrt{6}$ and hence the FWHM of the equivalent Gaussian coincides with the FWHM of the transmission function since $\sqrt{8\ln 2/6} \simeq 1$. Imperfections in the collimators that define the slit width, the non-infinitesimal distance between the two counter-rotating choppers and the finite transmission of neutrons through the absorbing layers tend to make the actual transmission functions assume a more Gaussian shape. In some situations, the root mean square deviation of the real transmission function was found to be better expressed by $\sigma = FWHH/2\sqrt{\ln 2}$ [10], in which case, the gaussian equivalent would be $FWHM_{Gauss} \simeq \sqrt{2}FWHM_{trans}$. Previous ray-tracing simulations also seem to indicate this to be the case at TOFTOF instrument [3], which was then taken into account in the resolution calculations here presented.

scattered with energies between 1.65 meV and 69 meV (hence from -64 meV to +3.35 meV in energy transfer), at the expense of a loss in the elastic line intensity by a factor three.

Though this needs not necessarily to be the case, in most time-of-flight experiments the time window of acquisition is not set to be centered at the elastic line, but instead to start when the neutron pulse impinges on the sample, in which case the scattered neutron energies covered extend from very high energies (∞) to a minimum energy value defined by the time window size (which, in this case, would correspond to the maximum neutron time-of-flight to be measured). In this situation, a generally followed rule of the thumb is that of considering this maximum time-of-flight to be given by [11]

$$t_{\max} = 1.5 t_{1\text{el}} = 1.5 \sqrt{\frac{m}{2}} \frac{L_1}{\sqrt{E_i}} = 1.5 \frac{m}{h} L_1 \lambda_i \quad (2)$$

where $t_{1\text{el}}$ represents the time an elastically scattered neutron (of wavelength λ_i) takes to travel from the sample to the detector positions (separated by the distance L_1). Hence, in these cases, the frameoverlap ratio is determined by the speed of rotation of the chopper system and the wavelength of the neutron pulses incident on the sample, as the minimum integer satisfying the condition:

$$R \geq t_{\max(\text{s})} \frac{f(\text{rpm})}{30} = 1.26 \times 10^{-5} \lambda_{i(\text{\AA})} L_{1(\text{m})} f(\text{rpm}) \quad (3)$$

Figure 3 presents the regions (in f vs λ_i space) corresponding to the different frameoverlap ratios, as calculated from the expression above for TOFTOF ($L_1 = 4\text{m}$).

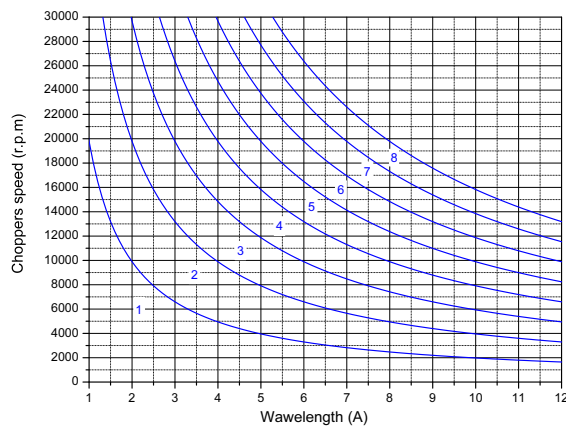


FIG. 3: Regions of different values of the frameoverlap ratio, in f vs λ_i space, as obtained from expression (3).

C. The detector system

TOFTOF's secondary spectrometer contains at the moment a total 605 He^3 cylindrical gas detectors, 522 mm long and of 25 mm diameter, squashed to have an almost rectangular section of 15×30 mm (figure 4) [12].

They are distributed over eight detector racks covering scattering angles between 7° and 140° (along the equatorial plane and the planes corresponding of a vertical component of the scattering angle of -7.8° , 7.8° and 15.6° - recall figure 1), and oriented so as to be tangential to surface of a sphere of radius 4.000 m centered at the sample position and to Debye-Sherrer circles that, in that sphere cover the scattering angles mentioned above.

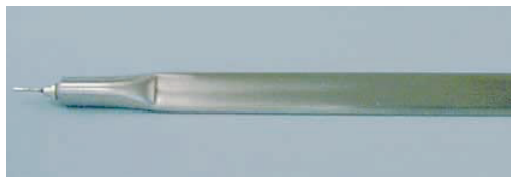


FIG. 4: Photograph of squashed detectors (from [12]).

There are detector performance parameters, such as the detector efficiency or the detector effective thickness, which depend on the energy of the detected neutrons. This results from the fact that neutrons are detected via absorption in the gas medium of the detector and that the absorption cross-sections vary linearly with the neutron wavelength in the wavelength range of interest, as shown in figure 5. So, unless all the neutrons to be detected have the same energy, the dependence of these parameters has to be properly accounted for, during instrumental performance analysis and data handling.

The neutron flux across a layer at a given depth x from the surface of a slab detector is given by:

$$n(x) = n_0 e^{-N\sigma_a(\lambda)x} \quad (4)$$

where n_0 represents the incident neutron flux and N is the density of absorbing atoms with neutron absorption cross-section $\sigma_a(E) = \sigma_0\lambda$ (see figure 5).

The absorption efficiency of a detector, defined by the fraction of neutrons entering the detector, which are actually absorbed by the detector material, is then, in the case of a slab detector of thickness d , given by:

$$\eta(d, \lambda) = \frac{n(d) - n(0)}{n(0)} = \left(1 - e^{-N\sigma_a(\lambda)d}\right) \quad (5)$$

with η depending on the wavelength of the detected neutrons through the wavelength dependence of the absorption cross-section of the detector material.

The detection efficiency is generally defined by the product of this quantity with another one, generally designated as neutron sensitivity. The latter represents the fraction of absorption events that result in an electric pulse from the detector. In the case of gas detectors, the neutron sensitivity is normally very close to unity, for a proper set up of the detector voltage and discriminator.

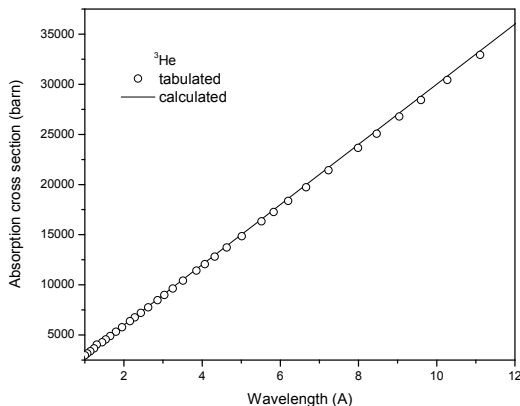


FIG. 5: Total absorption cross-section for ${}^3\text{He}$, as a function of neutron wavelength: scattered pointed tabulated values [13]; full line calculated from $\sigma_a(E) = \sigma_0\lambda$, with $\sigma_0 = 3000$ barn, for $\lambda = 1\text{\AA}$.

From equation (5) one can see that the efficiency value can be improved either by increasing the absorbers density or by increasing the detector thickness. Because of the first, gas detectors usually contain gas under pressure. For instance, the TOFTOF detectors are operated at 10 atm. As for the detector thickness parameter, wherever the time-of-flight technique is used, it affects also the instrument resolution, so any increase in detector thickness must be carefully evaluated.

The average detection position \bar{x} and an estimation of its uncertainty Δx (usually referred as *effective thickness*, can be obtained from the centroid and root mean square value of the $n(x)$ distribution, respectively. In the case of a slab detector of thickness d , the integrals:

$$\zeta_0(d, \lambda) = \int_0^d n(x)dx \quad \zeta_1(d, \lambda) = \int_0^d xn(x)dx \quad \zeta_2(d, \lambda) = \int_0^d x^2n(x)dx \quad (6)$$

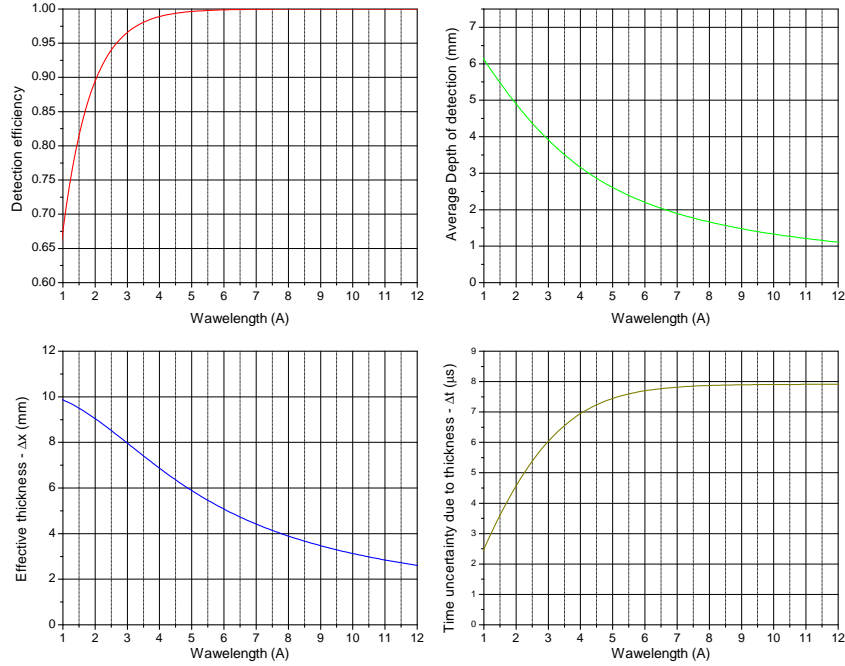


FIG. 6: Detection efficiency, detection average depth, effective thickness and detector thickness contribution to the total time uncertainty as a function of neutron wavelength. Calculated for detectors filled with ${}^3\text{He}$ at 10 atm ($N = 2.45 \times 10^{20} \text{ cm}^{-3}$ and $\sigma_a = 3000 \times 10^{-24} \lambda \text{ cm}^2$, for λ in \AA).

can be solved analytically² and hence \bar{x} and Δx are expressed by:

$$\bar{x}(d, \lambda) = \frac{\zeta_1(d, \lambda)}{\zeta_0(d, \lambda)} = \frac{1}{N\sigma_a} \frac{1 - e^{-N\sigma_a d}(1 + N\sigma_a d)}{1 - e^{-N\sigma_a d}} \quad (7)$$

² In the case of a detector with a circular cross section in the plane of the neutron beam, each slice of the circle at a distance z from the center will have a different thickness given by $d(z) = 2\sqrt{R^2 - z^2}$. In this case, expressions for the detector parameters can be obtained by proper averaging over z .

The detection efficiency is therefore given by:

$$\begin{aligned} \eta^*(R) &= \frac{1}{R} \int_0^R \eta(2\sqrt{R^2 - z^2}) dz \\ &= \int_0^1 1 - e^{-N\sigma_a 2R\sqrt{1-u^2}} du \end{aligned}$$

where $u = z/R$ and the integral can only be evaluated numerically.

Similarly, average detection position and effective thickness can be obtained numerically from:

$$\bar{x}^*(R) = \frac{\int_0^1 \zeta_1(2R\sqrt{1-u^2}) du}{\int_0^1 \zeta_0(2R\sqrt{1-u^2}) du}$$

$$\Delta x^*(R) = \sqrt{8 \ln 2} \sqrt{\overline{x^2}^*(R) - \bar{x}^{*2}(R)}$$

$$\text{with } \overline{x^2}^*(R) = \frac{\int_0^1 \zeta_2(2R\sqrt{1-u^2}) du}{\int_0^1 \zeta_0(2R\sqrt{1-u^2}) du}.$$

Nonetheless, since the TOF detectors are squashed detectors, they are here assumed to be well described as detectors of rectangular shape.

$$\Delta x(d, \lambda) = \sqrt{8 \ln 2} \sqrt{x^2(d, \lambda) - \bar{x}^2(d, \lambda)} \quad (8)$$

$$\text{with } \bar{x}^2(d, \lambda) = \frac{\zeta_2(d, \lambda)}{\zeta_0(d, \lambda)} = \frac{1}{N^2 \sigma_a^2} \frac{2(1 - e^{-N \sigma_a d} (1 + N \sigma_a d + \frac{N \sigma_a d^2}{2}))}{1 - e^{-N \sigma_a d}}.$$

The repercussion of the absorption cross-section dependence on the neutron wavelength on the η, \bar{x} and Δx functions of TOF/TOF detectors is shown in figure 6, together with the corresponding time-uncertainty, which represents the detector contribution to the total neutron pulse spread:

$$\Delta t = \frac{m \lambda_f}{h} \Delta x \quad (9)$$

where h stands for the Planck constant and m for the neutron mass.

An also important property of a detection system is its *dead-time*. This designates the maximum interval of time separating two absorption events that cannot be distinguished by the detector. In some cases the limiting time may be set by the processes in the detector itself, and in other cases the limit may arise in the associated electronics. In the case of the gas proportional counters it is mainly determined by the time involved in the drift of the electrons from a neutron absorption site to the anode. Hence, in these detectors, dead-time depends essentially on the counter cathode and anode diameters and on the chosen anode voltage [14, chap.4]. Typical values are of $\sim 1 - 2 \mu\text{s}$.

II. TIME-OF-FLIGHT, ENERGY TRANSFER AND MOMENTUM TRANSFER

As already mentioned, at time-of-flight spectrometers, as TOF/TOF, neutrons are counted as a function of their total flight time and conversion of this time scale to an energy transfer scale is later performed.

The total neutron flight time may be simply expressed by:

$$t = t_i + t_f = \frac{L_i}{v_i} + \frac{L_f}{v_f} = \sqrt{\frac{m}{2}} \left(\frac{L_i}{\sqrt{E_i}} + \frac{L_f}{\sqrt{E_f}} \right) \quad (10)$$

where $t_i, t_f, L_i, L_f, v_i, v_f, E_i$ and E_f represent the incident and scattered neutron flight times, flight path lengths, velocities and energies, respectively.

On the other hand, energy conservation law gives:

$$E = E_i - E_f \quad (11)$$

for E representing the energy transferred to the scattering system during the scattering process (or, by other words, the neutron energy loss).

Since on TOF/TOF spectrometer the incident energy is fixed by the chopper system, the scattered neutron energy can be substituted in equation (10) by $E_f = E_i - E$, giving the time-of-flight to energy transfer conversion expression:

$$E = E_i - \frac{m}{2} \frac{L_f^2}{\left(t - \sqrt{\frac{m}{2}} \frac{L_i}{\sqrt{E_i}} \right)^2} \quad (12)$$

Apart from the energy transfer, the neutron also transfers momentum to the sample, whose amplitude Q , can be calculated from the conservation law of momentum and the cosine rule:

$$\vec{Q} = \vec{k}_i - \vec{k}_f$$

$$Q^2 = 4\pi^2 \frac{2m}{\hbar^2} (E_i + E_f - 2\sqrt{E_i E_f} \cos 2\theta) \quad (13)$$

2θ being the scattering angle. This equation, together with the conservation law of energy determines the trajectories of a given measurement in the (Q, E) space. Figure 7 represents the dependence of these trajectories on 2θ and λ_i while, for the particular case to the elastic line, figure 8 represents some of the trajectories corresponding to the same value of Q in 2θ vs λ_i space.

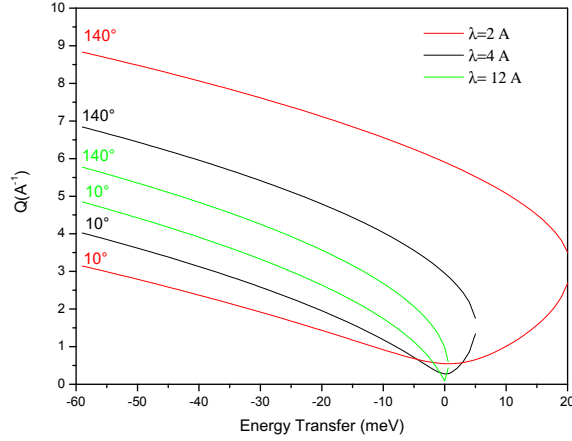


FIG. 7: Trajectories in (Q,E) space scanned with TOFTOF. Variation with scattering angle and incident beam wavelength.

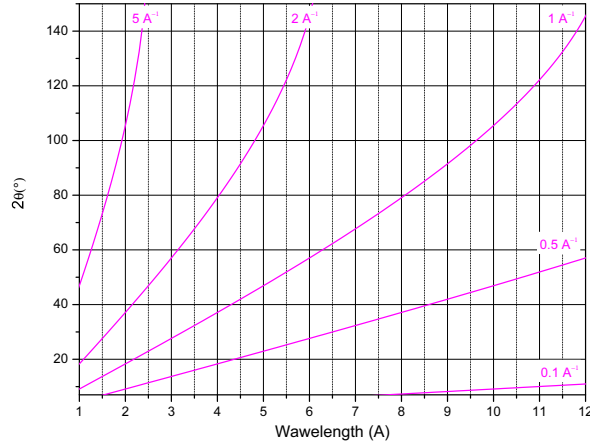


FIG. 8: Dependence of the momentum transferred in an elastic scattering process on the neutron incident wavelength and neutron scattering angle.

III. INSTRUMENT RESOLUTION

The distances and instants of time relevant for the evaluation of TOFTOF's resolution function are: $L_0=10.0$ m, the distance between the pulsing and monochromating pairs of choppers, $L_2=1.4$ m, the distance between the monochromating choppers and the sample position, $L_1=4$ m, the distance from the sample position to the detectors positions, t_p , the instant of departure of the neutron pulse from the pulsing pair of choppers, and t_m , t_s and t_d , the instants of arrival of the pulse at the monochromating pair of choppers, sample and detector positions, respectively.

The arrival time t_s of the pulse at the sample may then be expressed in terms of the prior instants of time and distances as

$$t_s = t_p + \frac{L_0 + L_2}{v_0} = t_p + (t_m - t_p) \frac{L_0 + L_2}{L_0} = \left(1 + \frac{L_2}{L_0}\right) t_m - \left(\frac{L_2}{L_0}\right) t_p \quad (14)$$

After the scattering process the neutrons travel a distance $L_1 = 4.0$ m, from the sample to the detector, the scattered neutron energy being determined by its flight-time $t_f = t_d - t_s$. Expression (12) can then be re-written as:

$$E = \frac{1}{2}m \left\{ \frac{L_0^2}{(t_m - t_p)^2} - \frac{L_1^2}{\left[t_d - \left(1 + \frac{L_2}{L_0}\right)t_m + \left(\frac{L_2}{L_0}\right)t_p\right]^2} \right\} \quad (15)$$

and the uncertainty ΔE can be obtained within a reasonable approximation from

$$\Delta E = \sqrt{\sum_x \left(\frac{\partial E}{\partial t_x} \Delta t_x \right)^2} \quad (16)$$

where Δt_x represents the uncertainties associated with each of the time instants. Hence, one obtains³:

$$\Delta E = 2\sqrt{\frac{2}{m}} \sqrt{\left(\frac{E_i^{\frac{3}{2}}}{L_0} + \frac{L_2}{L_0} \frac{E_f^{\frac{3}{2}}}{L_1} \right)^2 (\Delta t_p)^2 + \left(\frac{E_i^{\frac{3}{2}}}{L_0} + \left(1 + \frac{L_2}{L_0}\right) \frac{E_f^{\frac{3}{2}}}{L_1} \right)^2 (\Delta t_m)^2 + \left(\frac{E_f^{\frac{3}{2}}}{L_1} \Delta t_d \right)^2} \quad (17)$$

with $E_f = E_i - E$. The uncertainties Δt_p and Δt_m are given by the opening times of the pulsing and monochromating pairs of choppers and Δt_d is obtained from the convolution of all the time uncertainties associated with the performance of the detectors (dead-times, uncertainty in detection position) with the uncertainties in the scattered neutrons flight-path. Here, Δt_d was considered to be given by the convolution of a detection dead-time of $1\mu\text{s}$ with the time-uncertainty associated with the uncertainty in detection depth (expression (9)) and the time uncertainties resultant from the other two coordinates representing the detection position (due to the effective length and diameter of the detectors)⁴.

Expression (17) can be written in a more intuitive way as:

$$\Delta E = 2\sqrt{\frac{2}{m}} \frac{E_f^{\frac{3}{2}}}{L_1} \Delta t \quad (19)$$

where Δt is given by:

$$\Delta t = \sqrt{\left[\left(\frac{E_i}{E_f} \right)^{\frac{3}{2}} \frac{L_1}{L_0} + \frac{L_2}{L_0} \right]^2 (\Delta t_p)^2 + \left[\left(\frac{E_i}{E_f} \right)^{\frac{3}{2}} \frac{L_1}{L_0} + \left(1 + \frac{L_2}{L_0}\right) \right]^2 (\Delta t_m)^2 + (\Delta t_d)^2} \quad (20)$$

In figure 9, the uncertainty ΔE associated with each value of the neutron energy transfer E is represented for some particular choices of neutron chopper velocity and incident energy, together with the corresponding resolution function $\Delta E/E$. For one set of parameters ($\lambda = 4 \text{ \AA}$, choppers speed 20000 rpm, large slits for both monochromating and pulsing pairs of choppers) the individual contributions are also displayed. One can see that the major contributor to the instrument resolution is the monochromating CR pair of choppers. The contribution from the pulsing pair of choppers only dominates in the region of neutrons energy loss. The contribution of the secondary part of the spectrometer is generally smaller than that of the primary part of the spectrometer (when using large slits), except for situations of both high wavelengths and high chopper speeds, in the region around the elastic line.

The use of the smaller slits at the pulsing and monochromating pairs of choppers, would reduce the contribution of the primary part of the spectrometer to half its value while keeping constant the contribution from the secondary part of the spectrometer. It should be noted, however, that an almost equal resolution improvement can be obtained (at the elastic line and over the entire energy gain region) by keeping the large slits in use at the pulsing pair of choppers and only changing for the smaller slits at the monochromating pair of choppers.

Specifically with regards to the expected FWHM of the elastic line, the results are summarized in figure 10 and 11, once again for the option of using the largest chopper slits. In Figure 10 the dependence of the resolution at the elastic line, and its partial contributions, on both the wavelength and the choppers speed is presented. One can observe the increasing importance of the contribution from the secondary part of the spectrometer to the resolution at the elastic line, as both wavelength and choppers speed increase. In Figure 11 some of the isoresolution curves in choppers speed vs wavelength space are represented.

³ Note that this expression is equivalent to that presented R E Lechner [11].

⁴ These quantities may be estimated from:

$$\Delta t = \sqrt{\frac{m}{2}} \frac{\Delta L_1}{\sqrt{E_f}} \quad \Delta L_1 = L_1 \left(\frac{1}{\cos(\tan^{-1} \frac{x}{2L_1})} - 1 \right) \quad (18)$$

where $E_f = E - E_i$, x represents either the effective length (400 mm) of the effective width of the detector (30 mm), and $L_1 = 4 \text{ m}$. In the calculations presented the uncertainty due to the finite detector width was disregarded and only the uncertainty due to the detector length was considered, since the former was one order of magnitude smaller than the latter.

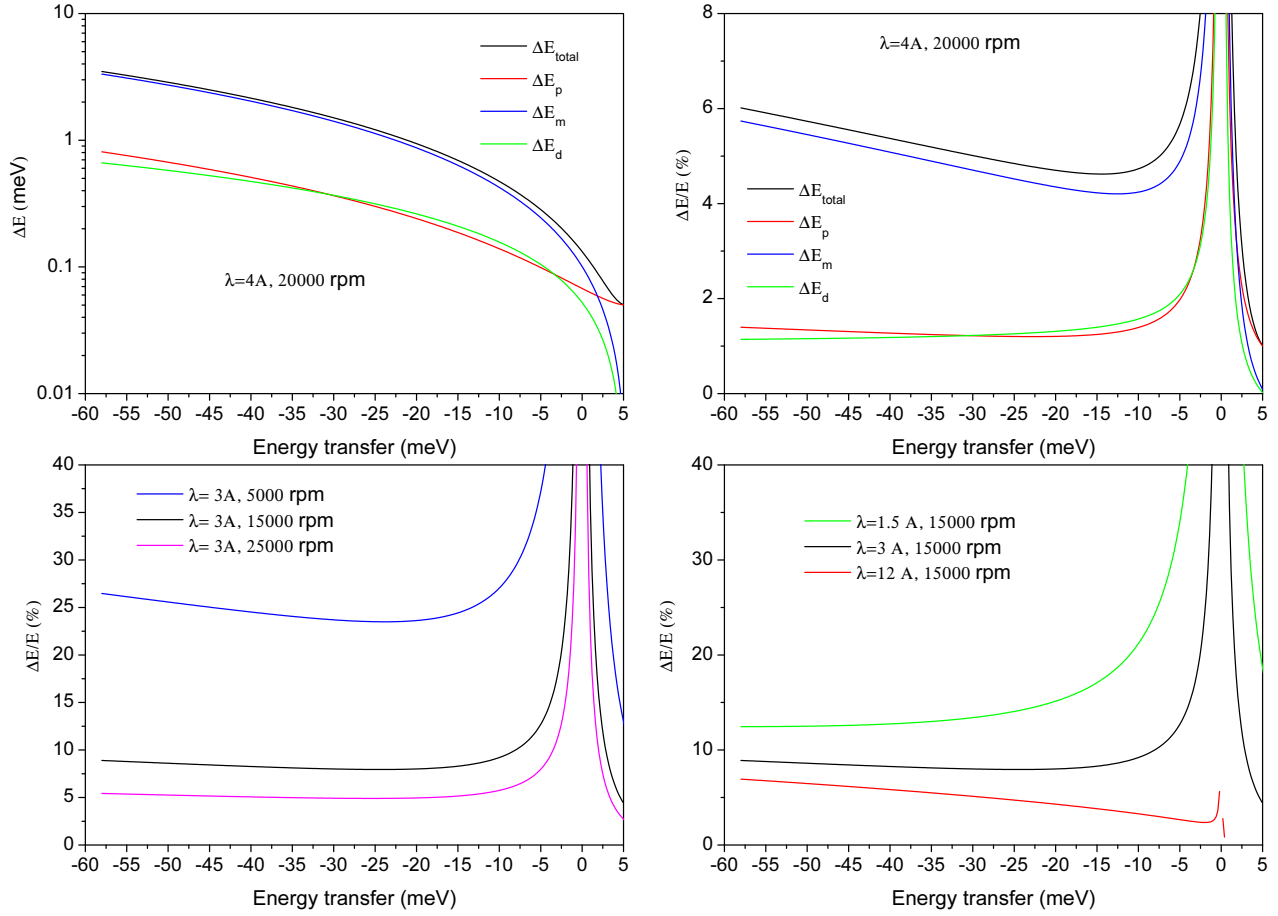


FIG. 9: TOP: Uncertainty in energy transfer and resolution of TOFTOF spectrometer for an incident neutron wavelength of 4\AA (and a choppers speed of 20000 rpm): total and partial contributions. BOTTOM: Variation of the instrument resolution with wavelength and choppers speed. Calculations performed considering the use of the larger set of slits.

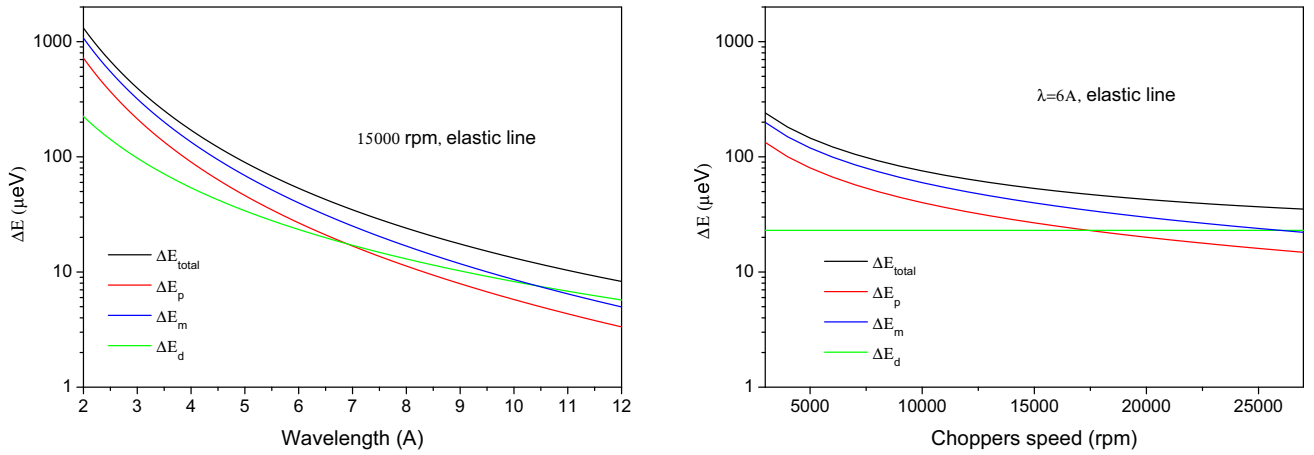


FIG. 10: Dependence of the energy uncertainty at the elastic line on the neutrons wavelength and choppers speed: total and partial contributions. Calculations performed considering the use of the large slits.

It will be interesting to extensively compare the results of these predictions with experimental values, obtained from the determination of the FWHM of the elastic incoherent scattering peak of a vanadium sample. Preliminary results, based on the limited experimental data available up to now, indicate an excellent agreement. In any case it should be noted that discrepancies of the order of 10% between the values calculated here and those determined experimentally are to be expected, given the approximations involved in the calculations.

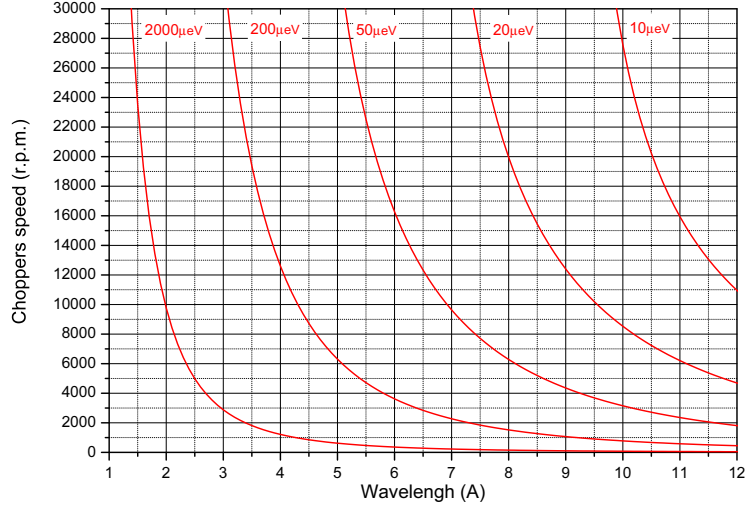


FIG. 11: Isoresolution curves at the elastic line in choppers speed vs wavelength space. Calculations performed considering the use of the large slits.

Another aspect that should be taken into account, when determining the resolution function corresponding to a specific measurement, is the sample dimensions, since they introduce uncertainties in the neutron flight-path. The corresponding time-spread will depend not only on the sample geometry, but also on the incident and scattered neutron energies, as well as on the scattering angle (2θ). For a rectangular sample of width $2c$ in the scattering plane and thickness $2a$, it will be given by: (figure 12):

$$\Delta t_s = \sqrt{\frac{m}{2}} \sqrt{c^2 \frac{(\sin 2\theta)^2}{E_f} + a^2 \left(\frac{1}{E_i} + \frac{1}{E_f} (\cos 2\theta)^2 - \frac{2 \cos 2\theta}{\sqrt{E_i E_f}} \right)} \quad (21)$$

c being typically a couple of centimeters, because of the neutron beam dimensions, and a being usually set to a value such that the multiple scattering contribution to the signal detected can be neglected (typically varying from some tenths of millimeter to some millimeters).

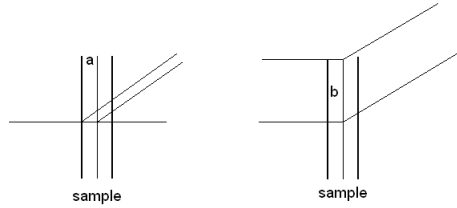


FIG. 12: The sample dimensions give rise to flight time spread.

On TOFTOF spectrometer, a sample with the geometry and dimensions mentioned above contributes to worsen the instrument resolution, at the elastic line, by at most 1% of the neutron incident energy.

This is not the case, however, for samples of cylindrical geometry for which an angle dependent resolution worsening is introduced, which may be particularly significant at high angles.

IV. INSTRUMENT INTENSITY

The intensity of an experiment is generally defined by the number of neutrons arriving at the sample position per unit time.

At TOFTOF, this quantity can be obtained multiplying the total number of neutrons transmitted through the chopper system with each pulse by the number of pulses per second arriving at the sample position n_p . The latter quantity is simply determined by the choppers speed and the frameoverlap ratio through

$$n_p = \frac{f_{(\text{rpm})}}{30} \frac{1}{R} \quad (22)$$

with R representing the frameoverlap ratio chosen.

The number of neutrons per unit wavelength transmitted each time a pulse is generated by the pulsing pair of choppers will be proportional to the neutron flux per unit wavelength arriving at their entrance, $d\phi/d\lambda_i$ (in $\text{n}/\text{cm}^2/\text{\AA}/\text{s}$), multiplied by the area of the choppers slits and by the choppers opening time Δt_p . The number of neutrons per pulse further transmitted by the monochromating pair of chopper will be then proportional to the ratio of the area of the choppers slits to the area of the neutron guide at their entrance⁵, multiplied by the wavelength band selected during the choppers opening time $\Delta\lambda_i = \frac{h}{mL_0} \Delta t_m$.

One may then write the following proportionality relation:

$$I \propto n_p b_p \Delta t_p b_m \Delta t_m \frac{d\phi}{d\lambda_i} \quad (23)$$

where Δt_m and Δt_p are given by expression (1) and b_p and b_m represent the widths of the pulsing and the monochromating chopper slits. Note also that, for purposes of clarity, the dependence of the instrument intensity on the quantities that are fixed at TOFTOF, such as L_0 , the heights of the chopper slits or the neutron guide dimensions, was not explicitly included in the expression above.

Further substitution of expressions (1) and (22) in expression (23), gives

$$I \propto b_p^2 b_m^2 f^{-1} R^{-1} \frac{d\phi}{d\lambda_i} \quad (24)$$

which expresses the instrument intensity dependence on the changeable instrument parameters, specifically, the widths of the pulsing and monochromating choppers slits b_p and b_m , the choppers system speed f , the wavelength chosen for the incident beam (through $d\phi/d\lambda_i$) and the frame overlap ratio chosen R .

Figure 13 represents some of the iso-intensity curves in wavelength versus choppers speed space, as calculated considering the regions of different frameoverlap ratio defined by expression (3) and the use of the larger slits in both pulsing and monochromating pairs of choppers. Note however that the numerical values displayed result from rough estimations (made on grounds not here discussed: the proportionality constant in expression (24)) and hence should be regarded as simply allowing to better understand the dependencies of the instrument intensity on the relevant instrument parameters, i.e. the wavelength of the incident neutrons, the choppers speed of rotation and the frame overlap ratio.

Note also that the secondary part of the spectrometer was not taken into account. This was because the number of neutrons per second detected at the instrument detectors will depend on the sample being used, while the number of neutrons arriving at the sample position per unit time is uniquely determined by instrument parameters. In addition, integration of the secondary part of the spectrometer necessarily introduces an additional degree of freedom, the scattered neutrons energy. Nevertheless, for the purposes of the evaluating of the statistical differences between acquisitions performed under different conditions at the same instrument, one should at least include the differences in the detectors efficiency for neutrons of different energies. Also when a comparison of the performance of two instruments is intended, it would probably be more adequate evaluating integrated intensity of the elastic line, detected at each of the instruments, with the same sample and for the same incident wavelength and resolution configuration. This would take into account not only the primary part of the spectrometers but also the secondary part of the spectrometers, namely the detector angular coverage.

⁵ In case of a parallel neutron beam, the area ratio to be considered should be that of the area of the monochromating choppers slits to the pulsing chopper slits.

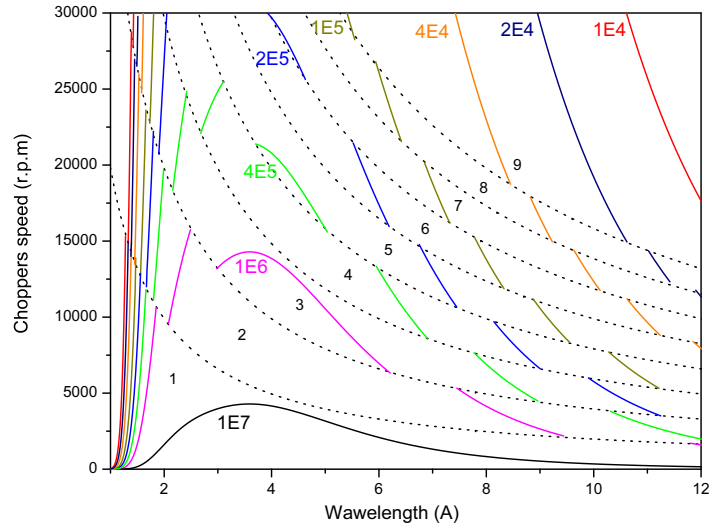


FIG. 13: Estimated elastic line isointensity curves in wavelength vs choppers speed space, considering the regions of different frameoverlap ratio values as defined by expression 3 and the use of the larger slits of both pulsing and monochromating pairs of choppers.

Final Note

To the advantage of the interested reader, the reference list of this manuscript is here extended to include additional documentation that, being related to the topics treated, was not explicitly cited in the text above [15, 16, 17, 18, 19, 20, 21].

Acknowledgments

This work was carried out under a short-term post-doc contract offered by the FRM II and further supported by a post-doc research grant (SFRH/BDP/17571/2004) attributed by Fundacao para a Ciencia e Tecnologia. The author gratefully thanks the continuous support and stimulus of the FRM II scientific director, Prof Winfried Petry. Dr Tobias Unruh, the TOFTOF's instrument scientist, is also acknowledged for finally motivating the publication of this study.

-
- [1] A. Zirkel, S. Roth, W. Schneider, J. Neuhaus, and W. Petry, *The time-of-flight spectrometer with cold neutrons at the FRM-II*, Physica B **276-278** (2000).
 - [2] A. Zirkel, Zwischenbericht uber den Bau des Flugzeitspektrometers mit kalten Neutronen am FRMII, Technical report, FRMII - Technische Universitat Muenchen, 2001.
 - [3] S. V. Roth, *Konzeption und neutronenoptische Optimierung des kalten Flugzeitspektrometers am FRMII*, PhD thesis, Technische Universitat Muenchen, 2001.
 - [4] TOFTOF webpage, http://www.frm2.tum.de/toftof/index_en.shtml.
 - [5] FRM II webpage, <http://www.frm2.tum.de>.
 - [6] S. Roth, A. Zirkel, J. Neuhaus, W. Schneider, and W. Petry, *Optimization of the neutron guide system for the time-of-flight spectrometer at the FRM-II*, Physica B **283** (2000).
 - [7] T. Unruh, J. Ringe, J. Drbecker, R. Funer, A. Gaspar, J. Neuhaus, and W. Petry, First commissioning steps at the time-of-flight spectrometer TOF-TOF at FRMII, Technical report, FRMII - Technische Universitat Muenchen, 2004.
 - [8] J. R. D. Copley, *On the use of multi-slot multiple disk chopper assemblies to pulse thermal neutron beams*, Nucl Instr and Meth Phys Res A **273**, 67–76 (1988).
 - [9] J. R. D. Copley, *Transmission properties of a counter-rotating pair of disk choppers*, Nucl Instr and Meth Phys Res A **303**, 332–341 (1991).
 - [10] C. G. Windsor, *Pulsed Neutron Scattering*, Taylor and Francis, 1981.

- [11] R. E. Lechner, TOF-TOF spectrometers at pulsed neutron sources and at steady-state reactors, Technical report, KEK reports 90-25, 1991.
- [12] A. C. inc., Helium-3 Squashed Neutron Detectors, <http://www.canberra.com/products/1139.asp>.
- [13] MCNP and ENDF nuclear data libraries, <http://atom.kaeri.re.kr/endlplot.shtml>.
- [14] P. A. Egelstaff, editor, *Thermal neutron scattering*, Academic Press Inc., 1965.
- [15] R. E. Lechner, *Optimization of the chopper system for the cold-neutron time-of-flight spectrometer NEAT at the HMI, Berlin*, Physica B **181**, 973–977 (1992).
- [16] R. E. Lechner, R. Melzer, and J. Fitter, *First QINS results from the TOF-spectrometer NEAT*, Physica B **226**, 86–91 (1996).
- [17] H. Schober, A. J. Dianoux, J. C. Cook, and F. Mezei, *Upgrade of the IN5 cold neutron time-of-flight spectrometer*, Physica B **276-278**, 164–165 (2000).
- [18] J. Ollivier, H. Casalta, H. Schober, J. C. Cook, P. Malbert, M. Locatelli, C. Gomez, S. Jenkins, and I. J. Sutton, *New perspectives on the IN5 time of flight spectrometer*, J Appl Phys A **74**, S305–S307 (2002).
- [19] J. Ollivier, M. Plazanet, H. Schober, and J. C. Cook, *First results from the upgraded IN5 disk chopper cold time-of-flight spectrometer*, Physica B **350**, 173–177 (2004).
- [20] J. R. D. Copley and J. C. Cook, *The Disk Chopper Spectrometer at NIST: a new instrument for quasielastic neutron scattering studies*, Chem Phys **292**, 477–485 (2003).
- [21] J. R. D. Copley, *An acceptance diagram analysis of the contaminant pulse removal problem with direct geometry neutron chopper spectrometers*, Nucl Instr and Meth Phys Res A **510**, 318–324 (2003).